Quantitative Bond Energetics in Atomic-Scale Junctions

Sriharsha V. Aradhya,[†] Aileen Nielsen,[†] Mark S. Hybertsen,[‡,*] and Latha Venkataraman[†,*]

[†]Department of Applied Physics and Applied Mathematics, Columbia University, New York, New York, United States, and [‡]Center for Functional Nanomaterials, Brookhaven National Laboratory, Upton, New York, United States

ABSTRACT A direct measurement of the potential energy surface that characterizes individual chemical bonds in complex materials has fundamental significance for many disciplines. Here, we demonstrate that the energy profile for metallic single-atom contacts and single-molecule junctions can be mapped by fitting ambient atomic force microscope measurements carried out in the near-equilibrium regime to a physical, but simple, functional form. We extract bond energies for junctions formed through metallic bonds as well as metal–molecule link bonds from atomic force microscope data and find that our results are in excellent quantitative agreement with density functional theory based calculations for exemplary junction structures. Furthermore, measurements from a large number of junctions can be collapsed to a single, universal force–extension curve, thus revealing a surprising degree of similarity in the overall shape of the potential surface that governs these chemical bonds. Compared to previous studies under ambient conditions where analysis was confined to trends in rupture force, our approach significantly expands the quantitative information extracted from these measurements, particularly allowing analysis of the trends in bond energy directly.

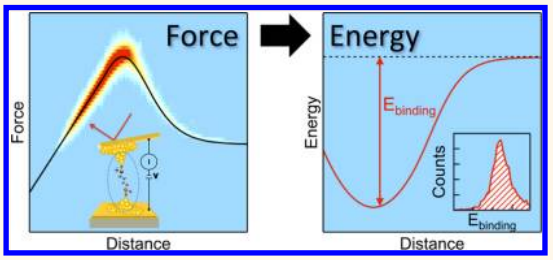

KEYWORDS: atomic force microscopy · single-molecule junction · chemical bond energy · force spectroscopy

Determining the strength and shape of short-range potential energy surfaces that characterize individual chemical bonds in complex systems is of fundamental importance. This challenging problem has motivated significant developments in atomic force microscopy (AFM)-based experiments over the past decade.[1−13] Examples include measurements of bond rupture forces in soft biological materials,[1,5] forces required to move atoms on surfaces,[3,7] forces sustained by a single molecule–metal junction under applied stress[4,11,13] and measurements that identify different atomic species on surfaces.[6,9] Extracting any information from these experiments about the underlying short-range potential energy profiles that control bond formation and rupture has not been straightforward. This is partly because experiments measure either force or change in force induced by the potential; energies must then be obtained from one (or two) integration of force (or stiffness) *versus* distance measurements. Also, thermal and mechanical instabilities confound bond energetics with other physical phenomena of the system. In cases where energy is lost to dissipation during the measurements, integration of force or stiffness curves cannot yield the correct short-range potential energy profiles even in principle. An alternative approach involves fitting part of the force curves that measure long-range interactions with model potentials that often have a large number of parameters.[12] Although such analysis does provide some energetic information[10,13] about the long-range molecule–surface interaction, obtaining molecule–metal bond energies through measurements of short-range forces has so far been inaccessible. Chemical trends have been determined,[11] but the underlying potential profile and its dependence on the distribution of specific structures probed for the short-range chemical-bonding regime have not been carried out.

Here, we examine the characteristics of a series of chemical linker bonds in nanoscale junctions including metallic single-atom contacts and single-molecule junctions formed through donor–acceptor bonds. In addition, some cases show a significant contribution from nonspecific interactions attributed to van der Waals (vdW) interactions at short length scale. We present a method to determine short-range

* Address correspondence to lv2117@columbia.edu; mhyberts@bnl.gov.

Received for review May 24, 2014 and accepted June 19, 2014.

Published online 10.1021/nn502836e

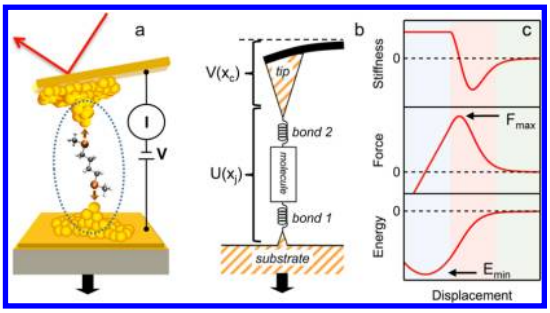

Figure 1. (a) Schematic illustrating the experimental setup. (b) Schematic illustrating the total mechanical model of the junction together with the AFM cantilever. (c) Representative potential energy (bottom panel), force (first derivative, middle panel), and stiffness (second derivative, top panel) as a function of elongation, illustrating the relationship between them. The physical regimes in these curves are the harmonic region near the energy minimum (blue), the maximum force region near the inflection (red), and the asymptotic region (green).

energy profiles quantitatively using simultaneous measurements of force and conductance carried out with AFM and focusing on the final connecting bond prior to rupture at a length scale that is typically 0.1 to 0.2 nm). We do not consider long-range vdW interactions explicitly, as these are only weakly distance dependent in the physical regime of our experimental setup. Thus, this work highlights a force regime that is fundamentally different from the generally longer range forces that have been studied previously.[13]

Our experiments measure conductance and force simultaneously (Figure 1a). The conductance data are used to identify the junction. The force measurement as a function of elongation probes a mechanical model of the junction (Figure 1b and c). Our experiments are performed in a regime where in principle the full force−extension curve could be probed. In practice, for each individual junction, a finite segment of the force−extension is measured and the energy profile as a function of elongation (Figure 1c) is reconstructed from the force data through a fitting procedure. In particular, we demonstrate that energy profiles for individual junctions can be parametrized by just two numbers, the bond energy and a length scale. Since this AFM-based measurement procedure provides an ensemble of individual junctions with diverse local structures at the nanometer scale near the linker bonds, our measurements provide distributions of bond energies as well as length scales for each type of bond probed. We show further that the complex and rich ensemble of data measured here can be rationalized through a scaling analysis that collapses complete experimental data sets onto a single universal force extension curve. This analysis enables us to visualize how potential energy profiles are sampled in the measurements, giving us some insight into the mechanics of individual atomic-scale junctions. The generality of this approach is demonstrated by analyzing Au and Ag single-atomic contacts as well as seven different molecular junctions formed by five molecules that bind to Au electrodes through donor−acceptor bonds and, in some cases, additional nonspecific, short-range interactions due to vdW. It is also applied to published calculations and measurements from other groups. Overall, we find excellent quantitative agreement with density functional theory (DFT)-based calculations for exemplary junction structures and also capture the microscopic diversity inherent to complex systems at nanostructured interfaces.[4,11,14,15] This technique significantly expands the ability of atomic force microscopy to quantify binding energetics at the atomic scale and to measure the diversity of bond strength at interfaces with nanostructured materials.

RESULTS

Figure 1 presents a schematic of the AFM used here, which has been described in detail previously,[11,15] and a corresponding mechanical model. Briefly, in the experiments, molecular or metal junctions are formed by repeatedly bringing the AFM cantilever probe in and out of contact with the substrate while measuring the junction conductance and the force across the junction in ambient conditions. Conductance provides a signature for the nature of the contact as it decreases stepwise in integer multiples of G_0, showing how the metal contact is thinned down to the single-atom scale. When the single-atom contact is broken in an environment of molecules terminated with chemical linkers, such as methyl sulfides, amines, or pyridine groups, which all bind selectively to the Au electrodes,[16] an additional conductance plateau at a molecule-dependent value is often observed. These plateaus indicate the formation of a single-molecule junction. We note here that when dithiol-terminated molecules are measured, the conductance signatures are not well-defined, and thus simultaneously measured forces cannot be analyzed with our method. The covalent nature and necessarily high binding energy of the Au−thiol bond means that almost all Au−thiol force measurements and associated bond ruptures are accompanied by substantial rearrangements of Au atoms in the electrodes.[17,18] Hence we do not fit data for single-molecule force measurements of molecules with Au−thiol linkers.

Figure 2a and b show sample measurements of conductance (upper panel) and force (lower panel) for a Au point contact (no molecule) and a Au-1,4-bis(methylthio)butane-Au (C4SMe) single-molecule junction. Additional data are shown in the Supporting Information (SI), Figures S6 and S7. The conductance traces show plateaus, while the simultaneously measured force shows a sawtooth pattern. Each linear force ramp is indicative of elastic stretching with a characteristic stiffness (the slope of this ramp). Sharp drops in force correspond to abrupt events involving junction

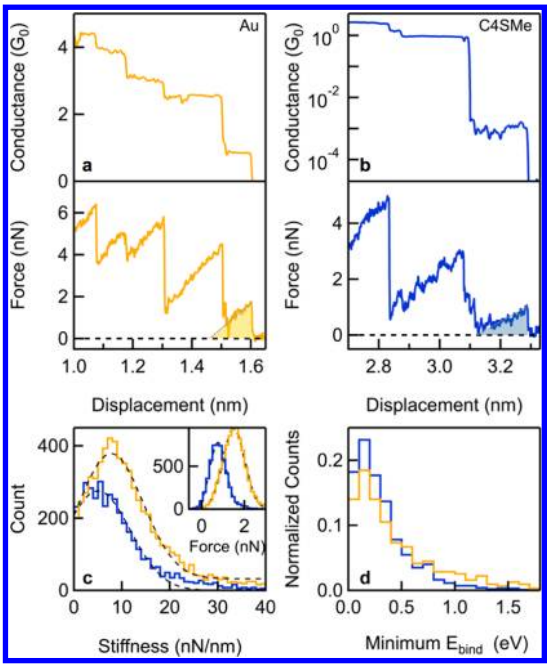

Figure 2. Measured conductance (upper panel) and force (lower panel) trace for a Au point contact (a) and a C4SMe junction (b). Triangles highlight the area under the force curve for the last rupture event. (c) Histograms of measured stiffnesses and rupture forces (inset) for the Au single-atom contact (yellow) and the C4SMe junction (blue). (d) Histogram of minimum binding energies (yellow for Au and blue for C4SMe) estimated by integrating the area under the last rupture event as shown in (a) and (b).

rearrangements and bond rupture.[14,15] The characteristics of the final connecting bond, the junction stiffness, and rupture force determined from the final segment of each measured trace (see SI) are compiled into histograms in Figure 2c for the Au single-atom contacts and for C4SMe junctions along with Gaussians fits, which are peaked at 1.5 and 0.8 nN, respectively, consistent with past measurements.[17,19] Force and stiffness results for five other junction types are shown in Figures S8 and S9.[14,17] The peaks of these distributions provide the most probable junction rupture force (or stiffness) for each junction type. Their widths, which are larger than the instrumental force resolution (~0.1 nN), are representative of intrinsic junction-to-junction variations. Such variations are found even in measurements carried out at 4.2 K in a vacuum.[14]

To determine the energy required to break the final connecting bond in these junctions, one could in principle integrate the force curve between appropriately chosen limits (Figure 1c). For example, consider integration backward from the rupture point down to zero force, which will usually involve extrapolating to the zero-force point from a linear fit to the force curve. Effectively, this method computes the area illustrated by the shaded triangles in Figure 2a and b. We show, in Figure 2d, the distributions of energies obtained for the Au single-atom contacts and for C4SMe junctions with this method. There is little difference between the two distributions, indicating that this method cannot distinguish between substantially different chemical bonds. Furthermore, the distributions shown in Figure 2d are peaked at very low energies, showing that direct integration of this segment of the force curves does not capture the full energy profile. This is not surprising. Even if the measured rupture force were to be close to the maximum sustainable force on the bond potential surface, that point is still far from the asymptotic regime of zero interaction energy, so this method must underestimate the binding energy (Figure 1c). More generally, thermal fluctuations typically prevent force segments measured in ambient conditions from probing the full potential landscape.

To interpret the measured force–displacement traces further, we need to establish the regime in which these measurements are carried out.[20,21] To this end, we consider the total mechanical system studied here, as illustrated in Figure 1b. It consists of the junction represented by a potential energy $U(x_j)$, where x_j is the displacement of the junction, connected to the AFM cantilever, which provides an external harmonic loading potential $V(x_c)$ of stiffness k_c and displacement x_c. When k_c is small compared to the stiffness of the internal junction potential d^2U/dx_j^2, the cantilever traverses a large distance compared to the internal elongation of the junction in response to an applied force; that is, x_c is larger than x_j. In this regime, the junction ruptures due to an internal instability in the full system and at a force that depends explicitly on k_c and therefore does not represent an intrinsic property of the junction.[20,21] For the junctions under study here, d^2U/dx_j^2 is substantially less than k_c, as our measurements are carried out with cantilevers that have a stiffness in the range 50–100 N/m, while junction stiffnesses are around 10 N/m. Hence the cantilever traverses a very small fraction of the total elongation ($x_c \approx x_j/10$) in our force–extension measurement. Moreover, the high sensitivity of our instrument enables measurements of small forces with relatively high stiffness cantilevers.[22] In this regime, the junction can rupture at, before, or beyond the point of inflection in $U(x_j)$, which defines the maximum sustainable force for the junction. The exact location along $U(x_j)$ where each junction ruptures depends on many degrees of freedom, including the position of the molecule in the junction and the thermally induced movements of metal atoms associated with the rough Au electrode structures.[18] Despite this experimental challenge, the force measurements presented here are carried out in a regime in which the internal junction potential is directly mapped, as is shown by our energetic analysis below. Further evidence for the extensive energy landscape sampling of our measurements comes from the fact that bond rupture forces and other junction characteristics measured are generally independent of the rate at which the junctions are pulled apart.[23,24]

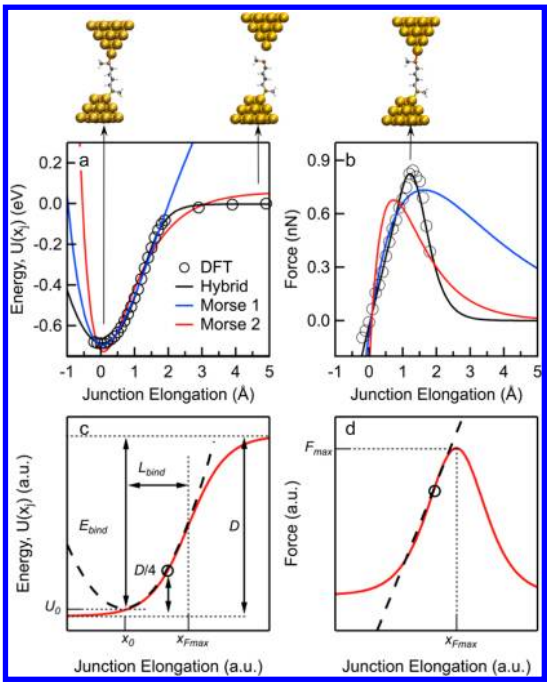

Figure 3. (a) DFT junction binding energy and structures for a Au−C4SMe−Au single-molecule junction (open circles) as a function of junction elongation. (b) Junction forces determined from the numerical derivative of the calculated DFT energies (open circles). In (a) and (b), the blue and red curves show the fit of the Morse potential to the harmonic region and the entire energy curve, respectively, while the black curve shows the fit of the hybrid model. (c) Schematic illustrating the construction of the hybrid model potential from separate harmonic (dashed black) and logistic (red) segments, including the energy, length scale, and connection point (circle). (d) The force profiles illustrate the linear harmonic regime (dashed black) and rupture regime (red) showing the maximum force point.

In principle, a direct integration of the force curve that follows the full potential landscape should yield the potential (Figure 1c).[25] In practice, as detailed above in the discussion of Figure 2, junctions form and rupture through a sequence of abrupt structural rearrangement events under continuous extension. As a consequence, a full force curve, starting from the potential minimum and ending in a well-defined asymptote characteristic of a single junction configuration, is not usually measured. Rather, the system often enters an elastic region of the trace under tension (beyond the potential minimum) due to the boundary conditions and then ruptures due to degrees of freedom other than the electrode displacement. We therefore require a model potential form to determine junction energetics from the measured forces.

For insight, we start from a DFT-based simulation of an exemplary junction. As described elsewhere, a C4SMe molecular junction is elongated adiabatically by moving the Au electrodes apart in small increments while minimizing the total energy at each step.[11,15,17,23] The total potential energy, $U(x_j)$, and the applied force, $F(x_j) = dU/dx_j$, determined as a function of the junction elongation (x_j), are shown in Figure 3a and b, along with snapshots of the junction structure along the trajectory. There is a clear elastic (harmonic) region around the potential energy minimum and a nonharmonic bond rupture region where the sustainable junction force has a maximum. Previous studies[12,13,26] have tried to model bond rupture using the pairwise Morse[27] and Lennard-Jones (LJ) potentials[28] or the universal binding curve derived to explain bulk metallic interactions.[29] We find, however, that none of these model potentials fit both the harmonic and bond rupture region of the DFT potential and force curves. For example, least-squares fits to the DFT-based potential energy profile with the Morse potential are shown in Figure 3a (and those for the LJ and the universal binding curve are shown in SI Figure S2). The derivatives of these least-squares fits are shown in Figure 3b. Significantly, the Morse potential does not fit either the shape or the magnitude of these force−extension curves. This may partly reflect the additional contributions, beyond stretching the sulfur−gold bonds, due to elastic distortions of the molecule and the gold tip structures as well as rotation of the molecule orientation.

To capture the mechanics of bond rupture at the atomic scale in an intuitive and analytically tractable fashion, we propose a new two-parameter hybrid model potential illustrated in Figure 3c. The model combines a harmonic segment, $U(x) = {}^1/_2K_{harm}(x - x_0)^2 + U_0$, near the energy minimum (dashed black curve) and a logistic segment, $U(x) = (D/(1 + e^{-(x-x_{Fmax})/r})$, for the bond rupture and asymptotic region (red curve). These curves were chosen to reflect two well-known force regimes: (1) a linear force-to-displacement relation to describe the near-equilibrium regime and (2) a nonlinear segment to capture bond rupture and the asymptotic zero force regime (discussed below). The harmonic region is characterized by a stiffness parameter K_{harm}, the equilibrium position x_0, and the energy minimum U_0. For the logistic segment, the parameter D controls the overall magnitude, the parameter r controls the scaling of the energy with displacement (the maximum force given D), and the parameter x_{Fmax} corresponds to the position of the force maximum (analytically $F_{max} = D/4r$). The distance from the equilibrium position to the force maximum, $L_{bind} = x_{Fmax} - x_0$, is an important internal parameter describing the model potential. The overall position on the distance scale, here taken to be x_{Fmax}, is not inherent to the model. However, it does position the model potential on a displacement axis relative to that of the measured force curve. The measured force curve does not start from a well-defined point along the potential, and x_{Fmax} must be included in the fitting procedure described below. Finally, the choice of energy zero does not enter the fitting. The binding energy is assigned to the difference between the asymptote of the logistic segment and the equilibrium energy for the harmonic segment ($D - U_0$).

The five internal parameters (K_{harm}, U_0, D, r, and L_{bind}) are reduced to two parameters (D and r) by application of three conditions. In particular, we combine the harmonic and logistic segments by requiring that they meet at a well-defined connection point; the precise choice of the connection point does not affect our results. We apply boundary conditions such that (1) the model potential is continuous and differentiable at the point that connects the harmonic potential to the logistic segment, (2) the tail of the logistic function is forced to go through the minimum energy point of the harmonic region, and (3) the curves join at a displacement where $U = D/4$. These boundary conditions provide us with three equations to reduce the physical parameters of the model to just D and r. With simple algebra (details shown in the SI), the parameters D and r can be used to determine the other physical parameters L_{bind}, K_{harm}, and E_{bind}, as well as the physically important F_{max}:

$$F_{max} = \frac{D}{4r} \quad (1)$$

$$K_{harm} = \frac{0.0804 \times D}{r^2} \quad (2)$$

$$E_{bind} = 0.9687 \times D \quad (3)$$

$$L_{bind} = 3.4310 \times r \quad (4)$$

The boundary conditions applied yield a transcendental equation, the solution of which results in the numerical values (dimensionless) that appear in eqs 2−4. In discussion below, we will characterize the fits in terms of E_{bind} and L_{bind}. For convenience, we also note that values of F_{max} and K_{harm} in units of nN and nN/nm, respectively, yield values of E_{bind} and L_{bind} in units of eV and Å, respectively, through simple relations:

$$E_{bind} = 7.78 \times \frac{{F_{max}}^2}{K_{harm}} \quad (5)$$

$$L_{bind} = 11.03 \times \frac{F_{max}}{K_{harm}} \quad (6)$$

Figure 3a presents the least-squares fit of this hybrid model to the DFT potential energy profile of C4SMe. The very good fit to the calculated energy demonstrates the ability of the hybrid model, despite its simple construction using just two parameters, to quantitatively capture all the essential features of the calculated potential. Figure 3b demonstrates the extremely good agreement between the derivative of the hybrid model fit and the DFT force profile. Finally, this hybrid model potential is similarly successful in describing all the atomic-size junctions for which we have made calculations for exemplary junction structures (Figures S3 and S4).

Our choice of the logistic segment as a flat approach to the asymptotic value at large distances naturally excludes the long-range contribution of vdW interactions.

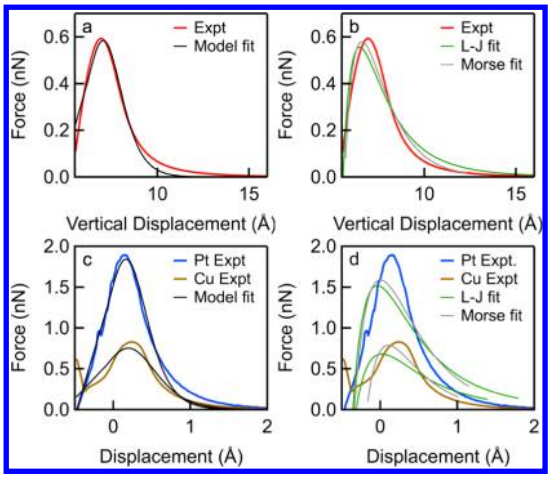

Figure 4. (a) Least-squares fit of the present hybrid model to force measurements of PTCDA in the molecular wire configuration, taken from Fournier *et al.*[30] (b) Least-squares fit of the LJ and Morse potentials for PTCDA in the molecular wire configuration. (c) Least-squares fit of the two-parameter model to force measurements of Pt and Cu atomic point contacts taken from Ternes *et al.*[10] (d) Least-squares fit of the LJ and Morse potentials for Pt and Cu atomic point contacts.

This is fully consistent with the DFT simulations in Figure 3, which disregard the extended tip and surface structure, as well as the long-range vdW interactions. In contrast to previous studies that start from the asymptotic regime and approach the surface at low temperatures,[13] we start with a well-formed chemical bond and elongate to rupture, an event that is typically well short of that asymptotic regime. Furthermore, in our regime, the typical force scale approaches 1 nN with noise under ambient conditions on the scale of 0.1 nN. We have simulated the impact of long-range vdW interactions between the tip and the substrate (Figure S5). We find that for the force−extension regime that covers the chemical bonding we probe, the long-range vdW contribution to the force is smaller than the typical noise scale noted (Figure S4). Finally, as a practical measurement protocol, we calculate our force by comparing measured force before and after the final rupture-force event, where the before and after are quite close in junction elongation. This effectively subtracts out the residual long-range vdW from beyond the point of rupture, also small compared to the typical noise scale.

Next, we perform a fit of our hybrid model potential to existing experimental data from the literature[10,30] and compare these fits to those of the LJ and Morse potentials. Figure 4a presents a fit of our model to AFM force measurements of a 3,4,9,10-perylene-tetracarboxylicacid-dianhydride (PTCDA) molecule in a free-standing molecule configuration on Ag from Fournier *et al.*[30] As the figure shows, our model closely follows the overall shape of the force event associated with pulling on the PTCDA molecule configuration and also captures the full magnitude of this force event. In contrast, as shown in Figure 4b, the Morse and LJ potentials fit this data poorly, failing to capture the

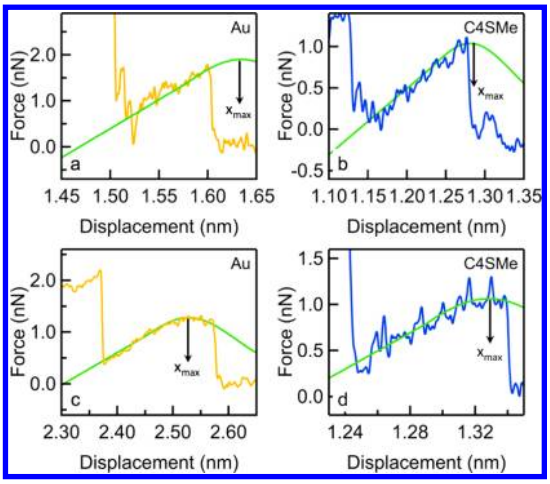

Figure 5. Example force traces fit with the present hybrid model for Au point contacts (a and c) and for C4SMe junction (b and d). Traces in (a) and (b) show junctions that rupture before reaching F_{max}, while those in (c) and (d) rupture after F_{max}.

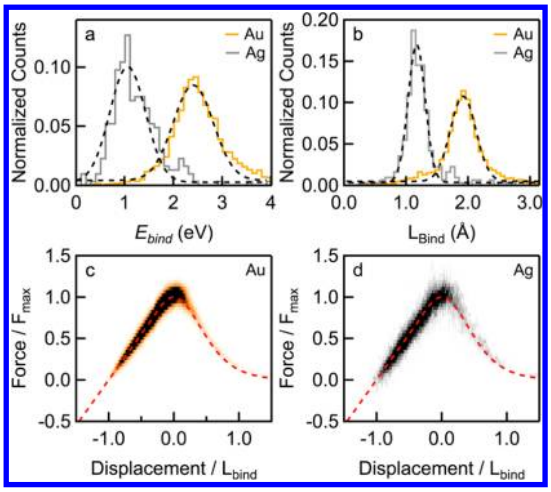

Figure 6. Histograms of experimentally determined (a) binding energy and (b) length scale using a two-parameter model to force curves for Au and Ag single-atom contacts. Two-dimensional histograms of scaled force curves for (c) Au single-atom contacts and (d) Ag single-atom contacts. The force profile determined from the hybrid model is overlaid (dashed red).

shape of the force trajectory and the magnitude of the rupture force. Similarly, we see in Figure 4c and d that our model also captures the shape and magnitude of rupture events of both Pt and Cu metallic single-atom contacts better than do the Morse and LJ potentials from Ternes *et al.*[10]

We now apply this model potential to fit the individual force extension curves measured with our ambient AFM setup. Because the junctions we measure start under tension and most likely not at the bond energy minimum, we need to determine three parameters rather than two, E_{bind} and L_{bind}, as in the examples above, but also the position of the potential relative to x_{Fmax} on the measured force extension curve at which our measurement begins. For this reason, we align the derivative of the potential on the measured force curve through a fitting parameter x_{Fmax}, which determines the location of F_{max} along the experimentally obtained position axis. The fitting of the experimental data with the model potential is done following a three-step procedure, as detailed in the Methods section, which allows a determinate of E_{bind} and L_{bind} for each experimental trace.

Figure 5 shows two sample experimental traces for a Au atomic contact junction and two for a C4SMe junction fit with this hybrid force profile. These junctions form under tension, at a nonzero force. In Figure 5a and b, the Au and C4SMe junctions rupture before x_{Fmax}; thus, the measured rupture force is smaller than F_{max}. In Figure 5c and d the junctions rupture beyond x_{Fmax}. In these junctions the measured rupture force is again smaller than F_{max}, but this is because the junction has gone beyond F_{max} into a regime where force attenuates with distance. As illustrated here, and in Figures S6 and S7 of the SI, breaking before or after F_{max} is statistically common.

We now fit all traces for different junction types to determine an E_{bind} and L_{bind} for each measurement, which are compiled into histograms. Figure 6a and b show these for Au and Ag atomic point contacts. The average binding energy determined for a Ag–Ag bond is 1 eV and that for a Au–Au bond is 2.4 eV, both in excellent agreement with published data.[31] The average length scale determined experimentally for these two contacts is 1.1 and 1.9 Å, which indicates that the extent of the potential for Ag is smaller than Au, again consistent with published calculations.[31] Furthermore, these histograms show physically reasonable variations in binding energy and length scale among the ensemble of junction structures realized. To show that all measured force traces are indeed well fit with our model potential, we can create a two-dimensional overlay of all measured force curves. We first normalize the force by the fitted F_{max} and the displacement by L_{bind}. We then shift each individual trace to have zero displacement at the fitted x_{Fmax} and thus create a two-dimensional overlay. Figure 6c and d show these scaled 2D plots for the Au and Ag atomic point contacts, respectively (see also Figure S12). These results show that thousands of individually measured force extension curves can be collapsed onto a single clearly defined universal force curve.

We use the same method to fit our model to 4,4′-bipyridine (BP) single-molecule junction force measurements where the molecule–Au interaction includes both a strong, nonspecific component (vdW-based) and a Au–N donor–acceptor bond. Conductance traces for BP junctions show two distinctive plateaus: a high conductance plateau where the molecule/Au interaction includes both the short-range vdW and donor–acceptor components at short electrode separations and a low conductance plateau corresponding to a fully elongated junction bound primarily through the

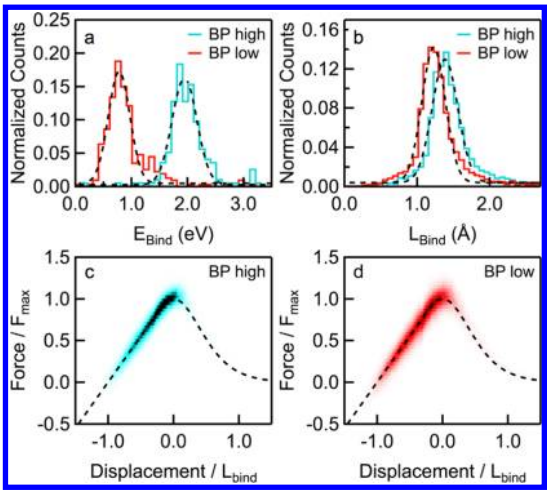

Figure 7. Histograms of experimentally determined (a) binding energy and (b) length scale using the two-parameter model to force curves for BP single-molecule junctions in the high- and low-conductance states. Two-dimensional histograms of scaled force curves for (c) BP high and (d) BP low. The force profile determined from the hybrid model is overlaid (dashed black).

TABLE 1. Most Probable Values of Experimental Binding Energies (E_{bind}) and Length Scales (L_{bind}) and Corresponding DFT Values

junction	n_{fit}	E_{bind} (eV)	L_{bind} (Å)	DFT E_{bind},[a] (eV)	DFT L_{bind}[a] (Å)
Au—Au	6114	2.4	1.9	2.1—2.8	
Ag—Ag	328	1.0	1.1	~1.5	
Au—C4SMe	2130	0.9	1.4	0.68	1.3
Au—C4A	553	0.9	1.4	0.65	1.2
Au—BDA	352	0.8	1.4	0.37	1.1
Au—BP_L	3989	0.9	1.2	0.81	1.2
Au—BP_H	2308	1.6	1.3	1.34[b]	
Au—BPE_L	342	0.7	1.0		
Au—BPE_H	203	1.9	1.5		

[a] From refs 11, 15, 17, and 31. [b] DFT parameters for BP_H junctions reported here were obtained from DFT calculations performed with a single Au electrode due to computational complexity.

donor—acceptor bond.[15,32] In Figure 7a and b we show the distributions of E_{bind} and L_{bind} for the two geometries. We find mean binding energies to be 0.73 and 1.8 eV for the low- and high-conducting junctions, respectively, in excellent agreement with calculated values.[15] As is physically intuitive, we see that the length scales of the two geometries are similar (1.2 and 1.3 Å), but the binding energy of the high-conductance geometry with its stabilizing van der Waals interactions is substantially higher than the binding energy of the low-conductance geometry. Despite the different origins of the interactions, we still see the same universal curve in the scaled 2D force map shown in Figure 7c and d.

Table 1 summarizes the most probable E_{bind} and L_{bind} for all the junctions measured (see Figures S8—S12) and compares it with calculated values where available.[11,15,17] The values determined for L_{bind} and E_{bind} are in excellent quantitative agreement with published DFT calculations where available. In the case of pyridine-linked junctions, our previous work demonstrated a key role for intermediate range van der Waals interactions.[15] Our present methodology implicitly captures this extra binding energy, and the results are in quantitative agreement with DFT calculations that include approximations of van der Waals interactions.[15,33]

The data for these single-molecule junctions show a remarkable similarity in shape and goodness of fit to the data from the atomic single-point contacts despite the very different chemical nature of these three interaction schemes. In all the scaled 2D maps, we see that our model force profile naturally passes through the data. As the intensity of the histogram indicates, the portion of the potential curve from modest initial tension to a point just beyond the inflection (force maximum) is most heavily sampled. However, a recognizable outline of the full curve emerges in the tails with lower data counts due to infrequently sampled ranges in the data. The clear emergence of a universal force—extension curve from the rescaled data not only reinforces the robustness and generality of the simple model but also reveals a surprising degree of similarity in the overall shape of the potential surface that governs bond rupture for metallic, donor—acceptor, and van der Waals interactions at the nanoscale.

CONCLUSIONS

We have demonstrated that AFM measurements carried out in the near-equilibrium regime with a stiff cantilever enable the complete mapping of the force—extension curve in nanoscale junctions under tension in ambient conditions. Our analysis, based on fitting a flexible, empirical potential form to those curves, reliably extracts physical characteristics of the potential energy surface that describes stretching and rupturing the bonds in each junction structure probed in the ensemble of measurements. Our scaling analysis of the full data set provides a clear picture of a universal potential describing the short-range interactions in the nanoscale junctions studied here. Our approach opens up the possibility to experimentally probe critical structure—bond energy relationships for molecules bonded to nanostructured materials where diverse structural motifs are an inherent feature.

METHODS

Experimental Details. We use a home-built conducting atomic force microscope to perform simultaneous conductance and force measurements on Au and Ag single-atomic contacts as well as Au—single-molecule—Au junctions. See SI Table S1 for a full list of junctions studied. The experiments are performed at

room temperature under ambient conditions. We use the break-junction procedure with our custom AFM and repeatedly bring the metal-coated AFM cantilever in and out of contact with the metal substrate. For measurements with Au, we use a Au-coated mica substrate, while for measurements with Ag we use a freshly polished Ag puck as the substrate.[34] Molecules are added on the substrate from solutions in 1,2,4-trichlorobenzene or phenyloctane, both obtained from Alfa-Aesar. The force constant of the AFM cantilever is determined using its thermal spectrum[35] at the end of each experiment. The experimental setup has been described in detail previously[11,36] and has been optimized for a high cantilever displacement resolution of ~2 pm between DC and 10 kHz, translating into a force noise of ~0.1 nN.

Data Analysis Details. We first analyze force events using an automated algorithm that has been described previously.[15] Once the last force event within a conductance plateau of interest has been identified, we fit a line to this rupture event to capture the junction stiffness. We also calculate the force from the sharp drop at the end of the force event. We fit the force trace of this last rupture event to the model using a three-step procedure. This is because of the highly nonlinear nature of the model as well as the fact that E_{bind} and L_{bind} enter the model through a linear and an exponential term, respectively. For each fitting step, one parameter is constrained to provide reliable fitting of the model to the experimental data on a trace-by-trace basis, as follows. First, a fit to determine x_{Fmax} is performed by constraining E_{bind} to the value obtained from eq 5 using the most frequent rupture force as F_{max} (the peak value from the measured distribution shown in Figure 2c) and the most frequently measured stiffness as K_{harm} (Figure 2c). The value obtained from this fit is $x_{Fmax,1}$. Next, a fit is performed by constraining L_{bind} to the value obtained from eq 6 above, and the value $x_{Fmax,2}$ is determined. Finally, a fit is performed by constraining x_{Fmax} to the average of $x_{Fmax,1}$ and $x_{Fmax,2}$. In this final fit, neither E_{bind} nor L_{bind} are constrained. To ensure that badly fit traces are not included in the analysis, fits that have a root-mean-square deviation greater than 0.15 nN (~1.5× instrumental force noise) from the data are not analyzed further. This fitting procedure allows a determination of E_{bind} and L_{bind} for each experimental trace.

Theoretical Details. The DFT-based calculations were performed using the generalized gradient approximation (GGA) of Perdew, Burke, and Ernzerhof (PBE)[37] implemented in the VASP package.[38] The contribution of van der Waals interactions was included in specific instances using the DFT-D2 method of Grimme,[33] implemented as a correction to the structures determined with PBE.[15] For each junction, a representative junction structure is considered with clusters to model the electrodes as shown in Figure 3. A potential energy surface is calculated as an adiabatic trajectory. The junction is elongated in small steps with geometry optimization at each step, as described previously for C4SMe, C4A, BDA, and BP.[11,15,36] As described in more detail in the SI, we analyze the impact of long-range vdW interactions on the experimental regime of the present measurements. Direct simulation of the interaction between the atomic-scale asperities captured by the model Au tip structures in Figure 3 and the extended surface on the opposite side shows a negligible effect. We model the interaction of the extended tip and surface as a hemisphere interacting with a planar surface and use the recently recommended value for C_6 that includes metal screening,[39] 80 eV-Å^6, likely most representative of the long-range component (Figure S5). We estimate an impact on the 0.1 nN scale or less over the range of the force– extension curve studied here (Figure S4).

Conflict of Interest: The authors declare no competing financial interest.

Acknowledgment. We thank the groups of Prof. Stefan Tautz (Jülich University, Jülich, Germany) and Dr. Markus Ternes (Max-Planck Insititute for Solid State Research, Stuttgart, Germany) for providing their raw data that was reproduced in Figure 4 here. This work was supported by the NSF Career Award CHE-07-44185 and the Packard Foundation. A portion of this work was performed using facilities in the CFN at BNL and supported by the DOE under contract number DE-AC02-98CH10886.

Supporting Information Available: Experimental details, model derivation, and additional data. This material is available free of charge *via* the Internet at http://pubs.acs.org.

REFERENCES AND NOTES

1. Grandbois, M.; Beyer, M.; Rief, M.; Clausen-Schaumann, H.; Gaub, H. E. How Strong is a Covalent Bond? *Science* **1999**, *283*, 1727–1730.
2. Lantz, M. A.; Hug, H. J.; Hoffmann, R.; van Schendel, P. J.; Kappenberger, P.; Martin, S.; Baratoff, A.; Guntherodt, H. J. Quantitative Measurement of Short-Range Chemical Bonding Forces. *Science* **2001**, *291*, 2580–2583.
3. Loppacher, C.; Guggisberg, M.; Pfeiffer, O.; Meyer, E.; Bammerlin, M.; Lüthi, R.; Schlittler, R.; Gimzewski, J.; Tang, H.; Joachim, C. Direct Determination of the Energy Required to Operate a Single Molecule Switch. *Phys. Rev. Lett.* **2003**, *90*, 066107.
4. Xu, B. Q.; Xiao, X. Y.; Tao, N. J. Measurements of Single-Molecule Electromechanical Properties. *J. Am. Chem. Soc.* **2003**, *125*, 16164–16165.
5. Fernandez, J. M.; Li, H. Force-Clamp Spectroscopy Monitors the Folding Trajectory of a Single Protein. *Science* **2004**, *303*, 1674–1678.
6. Sugimoto, Y.; Pou, P.; Abe, M.; Jelinek, P.; Perez, R.; Morita, S.; Custance, O. Chemical Identification of Individual Surface Atoms by Atomic Force Microscopy. *Nature* **2007**, *446*, 64–67.
7. Ternes, M.; Lutz, C. P.; Hirjibehedin, C. F.; Giessibl, F. J.; Heinrich, A. J. The Force Needed to Move an Atom on a Surface. *Science* **2008**, *319*, 1066–1069.
8. Albers, B. J.; Schwendemann, T. C.; Baykara, M. Z.; Pilet, N.; Liebmann, M.; Altman, E. I.; Schwarz, U. D. Three-Dimensional Imaging of Short-Range Chemical Forces with Picometre Resolution. *Nat. Nanotechnol.* **2009**, *4*, 307–310.
9. Gross, L.; Mohn, F.; Moll, N.; Liljeroth, P.; Meyer, G. The Chemical Structure of a Molecule Resolved by Atomic Force Microscopy. *Science* **2009**, *325*, 1110–1114.
10. Ternes, M.; Gonzalez, C.; Lutz, C. P.; Hapala, P.; Giessibl, F. J.; Jelinek, P.; Heinrich, A. J. Interplay of Conductance, Force, and Structural Change in Metallic Point Contacts. *Phys. Rev. Lett.* **2011**, *106*, 016802.
11. Frei, M.; Aradhya, S. V.; Koentopp, M.; Hybertsen, M. S.; Venkataraman, L. Mechanics and Chemistry: Single Molecule Bond Rupture Forces Correlate with Molecular Backbone Structure. *Nano Lett.* **2011**, *11*, 1518–1523.
12. Wagner, C.; Fournier, N.; Tautz, F. S.; Temirov, R. Measurement of the Binding Energies of the Organic-Metal Perylene-Teracarboxylic-Dianhydride/Au(111) Bonds by Molecular Manipulation Using an Atomic Force Microscope. *Phys. Rev. Lett.* **2012**, *109*, 076102.
13. Welker, J.; Giessibl, F. J. Revealing the Angular Symmetry of Chemical Bonds by Atomic Force Microscopy. *Science* **2012**, *336*, 444–449.
14. Rubio-Bollinger, G.; Bahn, S.; Agraït, N.; Jacobsen, K.; Vieira, S. Mechanical Properties and Formation Mechanisms of a Wire of Single Gold Atoms. *Phys. Rev. Lett.* **2001**, *87*, 026101.
15. Aradhya, S. V.; Frei, M.; Hybertsen, M. S.; Venkataraman, L. Van der Waals Interactions at Metal/Organic Interfaces at the Single-Molecule Level. *Nat. Mater.* **2012**, *11*, 872–876.
16. Park, Y. S.; Whalley, A. C.; Kamenetska, M.; Steigerwald, M. L.; Hybertsen, M. S.; Nuckolls, C.; Venkataraman, L. Contact Chemistry and Single-Molecule Conductance: A Comparison of Phosphines, Methyl Sulfides, and Amines. *J. Am. Chem. Soc.* **2007**, *129*, 15768–15769.
17. Frei, M.; Aradhya, S. V.; Hybertsen, M. S.; Venkataraman, L. Linker Dependent Bond Rupture Force Measurements in Single-Molecule Junctions. *J. Am. Chem. Soc.* **2012**, *134*, 4003–4006.
18. Kruger, D.; Fuchs, H.; Rousseau, R.; Marx, D.; Parrinello, M. Pulling Monatomic Gold Wires With Single Molecules: An Ab Initio Simulation. *Phys. Rev. Lett.* **2002**, *89*, 186402.

19. Rubio-Bollinger, G.; Bahn, S. R.; Agrait, N.; Jacobsen, K. W.; Vieira, S. Mechanical Properties and Formation Mechanisms of a Wire of Single Gold Atoms. *Phys. Rev. Lett.* **2001**, *8702*, 026101.
20. Evans, E. Probing the Relation between Force - Lifetime - and Chemistry in Single Molecular Bonds. *Annu. Rev. Biophys. Biomol. Struct.* **2001**, *30*, 105–128.
21. Friddle, R. W.; Podsiadlo, P.; Artyukhin, A. B.; Noy, A. Near-Equilibrium Chemical Force Microscopy. *J. Phys. Chem. C* **2008**, *112*, 4986–4990.
22. The displacement resolution is ~2 pm, yielding a force resolution of ~0.1 nN.
23. Kamenetska, M.; Koentopp, M.; Whalley, A.; Park, Y. S.; Steigerwald, M.; Nuckolls, C.; Hybertsen, M.; Venkataraman, L. Formation and Evolution of Single-Molecule Junctions. *Phys. Rev. Lett.* **2009**, *102*, 126803.
24. González, M. T.; Díaz, A.; Leary, E.; García, R. I.; Herranz, M. A. N.; Rubio-Bollinger, G.; Martín, N.; Agraït, N. S. Stability of Single- and Few-Molecule Junctions of Conjugated Diamines. *J. Am. Chem. Soc.* **2013**, *135*, 5420–5426.
25. Loppacher, C.; Guggisberg, M.; Pfeiffer, O.; Meyer, E.; Bammerlin, M.; Luthi, R.; Schlittler, R.; Gimzewski, J. K.; Tang, H.; Joachim, C. Direct Determination of the Energy Required to Operate a Single Molecule Switch. *Phys. Rev. Lett.* **2003**, *90*, 066107.
26. Trouwborst, M. L.; Huisman, E. H.; Bakker, F. L.; van der Molen, S. J.; van Wees, B. J. Single Atom Adhesion in Optimized Gold Nanojunctions. *Phys. Rev. Lett.* **2008**, *100*, 175502.
27. Morse, P. M. Diatomic Molecules According to the Wave Mechanics. II. Vibrational Levels. *Phys. Rev.* **1929**, *34*, 57–64.
28. Jones, J. E. On the Determination of Molecular Fields - II From the Equation of State of a Gas. *Proc. R. Soc. London, Ser. A* **1924**, *106*, 463–477.
29. Rose, J. H.; Ferrante, J.; Smith, J. R. Universal Binding-Energy Curves for Metals and Bimetallic Interfaces. *Phys. Rev. Lett.* **1981**, *47*, 675–678.
30. Fournier, N.; Wagner, C.; Weiss, C.; Temirov, R.; Tautz, F. S. Force-Controlled Lifting of Molecular Wires. *Phys. Rev. B* **2011**, 84.
31. Torres, J. A.; Tosatti, E.; Dal Corso, A.; Ercolessi, F.; Kohanoff, J. J.; Di Tolla, F. D.; Soler, J. M. The Puzzling Stability of Monatomic Gold Wires. *Surf. Sci.* **1999**, *426*, L441–L446.
32. Quek, S. Y.; Kamenetska, M.; Steigerwald, M. L.; Choi, H. J.; Louie, S. G.; Hybertsen, M. S.; Neaton, J. B.; Venkataraman, L. Mechanically Controlled Binary Conductance Switching of a Single-Molecule Junction. *Nat. Nanotechnol.* **2009**, *4*, 230–234.
33. Grimme, S. Semiempirical GGA-Type Density Functional Constructed with a Long-Range Dispersion Correction. *J. Comput. Chem.* **2006**, *27*, 1787–1799.
34. Aradhya, S. V.; Frei, M.; Halbritter, A.; Venkataraman, L. Correlating Structure, Conductance, and Mechanics of Silver Atomic-Scale Contacts. *ACS Nano* **2013**, *7*, 3706–3712.
35. Hutter, J. L.; Bechhoefer, J. Calibration of Atomic-Force Microscope Tips. *Rev. Sci. Instrum.* **1993**, *64*, 1868–1873.
36. Frei, M.; Aradhya, S. V.; Hybertsen, M. S.; Venkataraman, L. Linker Dependent Bond Rupture Force Measurements in Single-Molecule Junctions. *J. Am. Chem. Soc.* **2012**, *134*, 4003–6.
37. Perdew, J. P.; Burke, K.; Ernzerhof, M. Generalized Gradient Approximation Made Simple. *Phys. Rev. Lett.* **1996**, *77*, 3865–3868.
38. Kresse, G.; Furthmuller, J. Efficient Iterative Schemes for *ab Initio* Total-Energy Calculations Using a Plane-Wave Basis Set. *Phys. Rev. B* **1996**, *54*, 11169.
39. Ruiz, V. G.; Liu, W.; Zojer, E.; Scheffler, M.; Tkatchenko, A. Density-Functional Theory with Screened van der Waals Interactions for the Modeling of Hybrid Inorganic-Organic Systems. *Phys. Rev. Lett.* **2012**, *108*, 146103.